Injection molded microfluidic chips featuring integrated interconnects†

Dieudonne A. Mair,[a] Emil Geiger,[b] Albert P. Pisano,[b] Jean M. J. Fréchet[acd] and Frantisek Svec*[d]

Received 25th April 2006, Accepted 13th July 2006
First published as an Advance Article on the web 31st July 2006
DOI: 10.1039/b605911b

An injection molding process for the fabrication of disposable plastic microfluidic chips with a cycle time of 2 min has been designed, developed, and implemented. Of the sixteen commercially available grades of cyclo-olefin copolymer (COC) that were screened for autofluorescence and transparency to ultraviolet (UV) light, Topas 8007 × 10 was identified as the most suitable for production. A robust solid metal mold insert defining the microfluidic channels was rapidly microfabricated using a process that significantly reduces the time required for electroplating. No wear of the insert was observed even after over 1000 cycles. The chips were bonded by thermal fusion using different bonding conditions. Each condition was tested and its suitability evaluated by burst pressure measurements. The COC microfluidic chips feature novel, integrated, reversible, standardized, ready-to-use interconnects that enable operation at pressures up to 15.6 MPa, the highest value reported to date. The suitability of these UV transparent, high pressure-resistant, disposable devices was demonstrated by *in situ* preparation of a high surface area porous polymer monolith within the channels.

Introduction

Miniaturizing devices for biomedical analysis will lead to portable and self-contained point-of-care diagnostic tools. In addition to portability, efforts to scale-down chemical analysis with microfluidic devices are driven by the significant reduction in the volume of reagents and samples required for analysis as well as the acceleration of the process due to shorter distances the sample has to traverse. The microfluidic chips can be fabricated from a variety of materials including silicon, fused silica, glass, quartz, and plastics.[1] The chemistry of these substrates is well understood and most also have the optical properties that are required for detection by laser-induced fluorescence (LIF). The first micro total analytical system (μTAS) to be introduced[2] was made from inorganic materials because the micromachining processes developed for the fabrication of integrated circuits were readily adaptable. However, fabrication involved a multi-step process consisting of cleaning, mask deposition, lithography, and etching, which is both slow and expensive.[3] Therefore, a transition from the conventional substrates to plastics[4] would enable the cost-effective and high-volume production of disposable microfluidic devices. Today, the most common technologies for the preparation of microfluidic systems from plastics involve laser ablation,[5] hot embossing,[6] soft lithography,[7] or injection molding.[8] A wide variety of polymers such as polyimide, poly(methyl methacrylate), polycarbonate, poly(dimethylsiloxane), and polyolefins have already been used [9] with the choice of the specific material determined by its physical and chemical properties as well as the technology used for fabrication.

An obstacle that currently impedes broader use of microfluidics is the lack of standard interconnects for interfacing the macroscale environment with the microfluidic channels within the chip.[10–12] The issue of convenience is especially important in high-throughput applications where the time constraints involved with the manipulation of several interconnects can be large enough to offset the economic advantages of migrating to a microfluidic platform.[13] The failure of an individual interconnect can be detrimental to device operation and repair is often not an option. Although reports on the fabrication and use of microfluidic devices for analysis frequently omit their description, interconnects, are now receiving considerable attention and have been recently reviewed.[13] Typically, capillaries, tubes, and pipette tips are glued to the fluid access holes. Unfortunately, this manual approach depends on the skill of the operator and is not always reproducible.[10,14] Moreover, the use of glue may lead to chemical contamination.[15] Therefore, multistep interconnect fabrication techniques that bar the glue from contacting working fluids[10,16–19] as well as glue-free methods[20,21] have been developed.

Although these approaches address most of the problems associated with glue-based interconnects, they all lack an important feature: reversibility.[14] The need for reversible interconnects has led many to develop customized formats.[22–25] Lately, a standardized reversible PEEK fitting that is glued onto the chip face has been commercialized.[26–30] However, these fittings are costly and glue is again required for their attachment. As an alternative, others have developed docking stations that house the chip and that function as a socket through which all fluidic and electrical connections are made.[14,31]

[a]*Department of Chemical Engineering, University of California, Berkeley, CA 94720*
[b]*Department of Mechanical Engineering, University of California, Berkeley, CA 94720*
[c]*Department of Chemistry, University of California, Berkeley, CA 94720-8139*
[d]*The Molecular Foundry, Lawrence Berkeley National Laboratory, Berkeley, CA*
† The HTML version of this article has been enhanced with additional colour images.

This article describes the selection of a cyclic olefin copolymer (COC) material for the fabrication of chips with the desired optical transparency and its use in the development of micro-injection molding using mold inserts that enable the rapid and high-volume production of chip parts with integrated reversible ports, and finally the optimization of bonding by thermal fusion. Application of the chip is then illustrated with the preparation of a porous monolith and a chemically reactive interfacial skin directly within the channel of the chip *via* UV initiated polymerization.

Experimental

Optical properties

Substrates in the form of plaques were generously provided by Ticona (1.7 mm thick) and Zeon Chemicals (2.0 mm thick). A fluorimeter (HORIBA Jobin Yvon, Inc., Edison, NJ) was used to measure fluorescence from the front aperture using an excitation wavelength of 405 nm. A UV-vis spectrophotometer (Varian, Walnut Creek, CA) was used to measure transmission in the UV and deep UV (DUV) range. To facilitate the comparison of transparency for plaques of different thickness, the percent transparency T_2 of the material with a desired thickness l_2 was calculated using eqn (1)

$$T_2 = 100\left(\frac{T_1}{100}\right)^{l_2/l_1} \quad (1)$$

where T_1 and l_1 are the corresponding experimentally determined values.

Mold insert fabrication

A mold insert with positive raised features defining the cross sectional geometry and layout of the microfluidic channels was fabricated using a variation of the LIGA process.[32–35]

Substrate preparation. The 500 μm thick nickel sheet (UNS N02200, National Electronic Alloy, Inc., Santa Ana, CA) was cut into 100 mm diameter discs using wire electrical discharge machining (EDM). Next, the discs were thermally annealed at a reduced pressure of 94.5 kPa and oxygen-free atmosphere consisting of 20% hydrogen and 80% argon. Annealing began by heating the substrates from 200 °C to 1100 °C at 2 °C min^{-1}. After 2 h at 1100 °C, the disks were cooled to 200 °C at 2 °C min^{-1}. The annealed substrates were then individually flattened by placement between two ground parallel steel plates in a Baldwin 400 kip universal testing machine. Flattening the discs requires straining them slightly beyond the yield stress, which is 185 MPa for annealed Ni 200. Next the disc surface was polished to a mirror finish by chemical mechanical polishing (CMP) performed with a donated slurry (Cabot Microelectronics, Aurora, IL) at 480 g cm^{-2} for 15 minutes using a pad and wafer rotation rate of 50 rpm on a conventional rotary tool. The final roughness of the surface after CMP was 10 nm.

Lithography. Lithography was carried out in the Berkeley Microfabrication Laboratory. Adsorbed water was removed from the substrates by drying at 120 °C for 15 min and organic contaminants were removed *via* an oxygen plasma (300 W, 48 Pa O_2, 15 min). A negative-tone photoresist (SU-8 2075, MicroChem Corporation, Newton, MA) was spin-coated on the substrate using the static dispense method. After allowing the puddle of resist (4 mL) to settle for 20 s, the resist was spread (500 rpm, 20 s, 1 krpm s^{-1}) to achieve a continuous resist coating over the substrate prior to the final spin step (1500 rpm, 20 s, 1 krpm s^{-1}) which yields a final film thickness of 150 μm. Following the pre-exposure bake (70 °C, 5 min 95 °C, 20 min) the substrate was allowed to cool for 10 min by natural convection. Flood exposure at 365 nm with a dose of 254 mJ cm^{-2} (SUSS MicroTec Inc., Waterbury Center, VT) was followed by a post-exposure bake at 70 °C for 1 min and at 95 °C for 10 min followed by 10 min cooling. Development was carried out at room temperature using SU-8 developer for 10 min. Finally, the substrates were thoroughly rinsed with 2-propanol and water, dried and plasma cleaned as above. Contact hot plates were used for all heating steps in order to ensure reproducibility. The 2-stage heating and 10 min cooling steps are important for minimizing resist cracking and delamination from the substrate.

Wood's strike bath. The substrate was loaded in a custom made jig that isolates the non-plated regions from the bath. The jig-wafer assembly was then placed in a stirred Wood's strike (240 g L^{-1} $NiCl_2 \cdot 6H_2O$ and 160 g L^{-1} conc. HCl, 40 °C). A depolarized, soluble Ni anode (Alan Baker Co., South San Francisco, CA) was loaded in a canvas bag to prevent large particles of nickel from entering the solution. A constant current power supply (Keithley, Instruments Inc., Cleveland, OH) was used to maintain a current density of 100 A m^{-2} for 50 min, yielding a 5 μm layer of active nickel. After 50 min the power supply was turned off and the jig was carefully removed to ensure that a puddle of bath solution remained over the active area. Liquid must be maintained over the active area because the presence of nickel oxide is suspected to be responsible for poor adhesion between substrate and electrodeposited film.[36] After displacing this puddle from the wafer surface with deionized water the jig-wafer assembly was finally placed in the electroplating bath.

Electroplating. A layer of 100 μm Ni was electrochemically deposited at a current density of 100 A m^{-2} in a ready-to-use nickel sulfamate electroplating bath (Technic, Inc., Anaheim, CA). The heating element enclosed in a quartz sheath (Cole Parmer, Vernon Hills, IL) was controlled with a fuzzy PID controller to maintain the bath temperature at 40 °C. Simultaneous agitation and filtering was achieved using a pump fitted with a filter at the inlet (Flo King, Longwood, FL). The pump effluent was directed towards the center of the active plating area. The thickness of the electroplated layer was found to closely follow that calculated using Faraday's Law.

$$x = \frac{1}{\rho}\frac{m}{q}\frac{I}{A}t \quad (2)$$

where x is the film height, ρ is the density of nickel, I is the plating current, A is the surface area plated, and m and q are the mass and charge of one mole of nickel, respectively.

Resist stripping and dicing. After electroplating the photoresist was stripped for 4 h at 80 °C in a bath of SU-8 Remover (MicroChem). The substrate was then rinsed with isopropanol and water and then coated with a 8 μm layer of positive tone photoresist to protect the structures from being damaged by small particles generated during the dicing. The dicing tool (Disco Hi-Tec America Inc., Santa Clara, CA) was used to make aligned cuts yielding a mold insert with channel termination points or pads precisely aligned to the access holes on the mold base of the injection molding tool.

Injection molding

Chips were fabricated from COC pellets (Topas 8007 × 10, Ticona, Florence, KY) using a Roboshot 30α-I injection molding machine (FANUC America Corporation, Chicago, IL). A standard mold base (D-M-E Co., Madison Heights, MI) was machined in-house and polished (Elmers Mold Polishing and Repair, San Marcos, CA) to a mirror finish for the production of optically clear parts. The mold base was maintained at 80 °C during production using thin film resistive heaters (Therm-X, Hayward, CA) that were customized to accommodate the ejector pins and mounted behind the A- and B-side mold plates. Insulating sheets (D-M-E, Madison Heights, MI) were positioned behind the mold plates in order to limit the thermal mass. Injection speed, packing, and other molding parameters were optimized for part quality and reduction of cycle time.

Bonding

A hydraulic press (Carver, Inc., Wabash, IN) fitted with heated plates and an analog load gauge was used to thermally bond the chips. Customized Pyrex bonding plates were made to accommodate the protruding ports of the chip during the bonding process.

Burst pressure measurement

The burst pressure was measured by connecting the plastic device to a microLC pump (Micro-Tech Scientific, Vista, CA) fitted with a pressure transducer with an error accuracy of 0.5% over the range of 0–69 MPa. The voltage signal from the pressure transducer was transmitted through a voltage divider, recorded using ChromPerfect software, and converted to pressure using a calibration curve provided by the manufacturer. A computer was used to set the water flow rate at 1 μL min^{-1} and to record the signal from the pressure transducer. After pumping water through the device for 1 to 2 min, a plug fitting (Upchurch Scientific, Oak Harbor, WA) that blocked flow was threaded into the remaining I/O port of a single-channel device.

Preparation of a monolith within the channel of the plastic chip

Methyl methacrylate (99%, MMA), butyl methacrylate (99% BuMA), ethylene dimethacrylate (99%, EDMA), ethylene diacrylate (99%, EDA), 2,2-dimethoxy-2-phenylacetophenone (99%, DMPAP), benzophenone (99.9% BP), cyclohexanol, and 1-dodecanol were purchased from Aldrich (Milwaukee, WI). MMA, BuMA, and EDMA were vacuum distilled and all other chemicals were used as received.

The channel surface was first grafted with an adhesion layer of polymer as follows: a mixture of 0.485 g MMA, 0.485 g EDA, and 0.030 g BP was purged with nitrogen for 10 min and then pumped into the bonded chip using a gas tight 100 μL syringe (Hamilton Company, Reno, NV). The chip was then irradiated with the DUV light source (Optical Associates Inc., San Jose, CA) for 4 min, and subsequently flushed with several channel volumes of methanol.

The monolith was then prepared within the chip using a modification of the procedure developed previously in our group.[37] The surface modified channel was filled with a polymerization mixture comprised of 0.400 g EDMA, 0.600 g BuMA, 1.500 g 1-decanol, and 0.01 g DMPAP that had been purged with nitrogen for 10 min. Irradiation for 10 min and subsequent washing with methanol afford monolith with a pore size of 2.2 μm as measured using mercury intrusion porosimetry.

Results and discussion

Optical properties of COC

COC has become an increasingly popular choice for chip production because of its uniquely high transmission in the UV and DUV and low autofluorescence.[38–51] UV transparency is critical to the successful preparation of a porous polymer monolith directly within the channel of the chip *via* photoinitiated polymerization. Because wide variations in optical properties between samples from different vendors and even among samples from the same vendor have been reported,[52] we measured both the UV transparency and autofluorescence of all commercial grades of COC currently available.

The photoinitiated reactions leading to surface modification of the channel wall for covalent attachment of the monolith requires DUV light with a wavelength near 250 nm while the subsequent preparation of the monolith is carried out using near UV irradiation (λ = 300–400 nm). Therefore, we measured the UV and DUV transmission of several samples and then used eqn (1) to predict the transparency for a sample 1 mm in thickness. This normalization facilitated the comparison of samples of different thicknesses. Fig. 1 shows the UV transparency spectra obtained for all 16 grades of COC tested. The major source of variation among grades is the presence of various types and levels of small molecule additives such as flame-retardants, smoke suppressants, lubricants, antioxidants, and UV absorbers that are often benzophenone derivatives designed to mitigate UV-induced material damage. These additives are routinely added to commercial polymers to improve their processability and extend lifetimes. Given its relatively low UV transparency it is interesting that grade 1020R from Zeon is one of the more popular grades used for the preparation of chips containing monolith.[39,43,44,53]

The high level of autofluorescence observed for most polymers is a barrier to the universal transition from glass to plastic microfluidic devices because it significantly reduces the sensitivity of detection by LIF.[39,44,54,55] While low autofluorescence of COC has been previously reported,[42,52] the observed variation in UV transparency among various grades

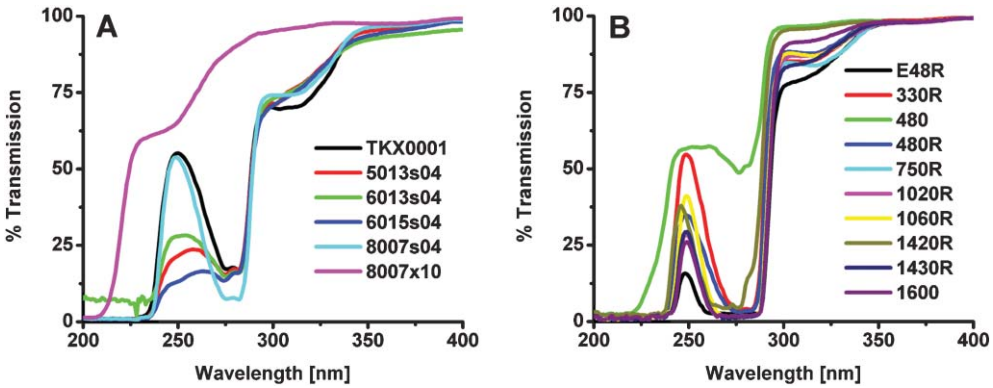

Fig. 1 UV and DUV transmission for several grades of COC from Ticona (A) and Zeon (B).

motivated us to measure the autofluorescence of each available COC grade. Because we plan to use fluorescamine (λ_{abs} = 405 nm, λ_{emis} = 500 nm) to label proteins for detection by LIF in our studies, substrates were excited at 405 nm and the intensity of the emission was collected from 420–700 nm. To facilitate comparisons with glass, the autofluorescence found for individual polymers is divided by that observed for glass.

Fig. 2 shows that the autofluorescence of selected COC materials varies considerably. Interestingly, all products of Zeon Chemicals have a low autofluorescence as indicated by fluorescence ratios ranging from 5 to 25 only. In contrast, some COC grades from Ticona show a fluorescence that exceeds that of glass by a factor of as much as 250 while others do not exceed 30. Again, the additives are the most probable source of variation in autofluorescence. Unfortunately, the presence of these unknown additives precludes a simple linearization of the fluorescence intensity to account for the 15% difference in thickness between the samples provided by the two vendors.[56] However, this difference in thickness is not expected to be large enough to entirely account for the 10-fold difference in fluorescence intensity.

Based on their low autofluorescence and high DUV transmission Topas 8007 × 10 from Ticona and Zeonex 480 from Zeon chemicals were identified as strong candidates for chip production. Despite its slightly larger autofluorescence, the Ticona polymer was chosen here for chip production for its superior transmission in the DUV region and lower T_g (80 °C *versus* 138 °C). The high transmission of Topas 8007 × 10 in the DUV region facilitates surface modification necessary for anchoring monolith to the channel walls and the lower T_g reduces the heat requirement for injection molding and chip bonding. Grade 480 from Zeon is more suitable for fabricating devices with integrated heaters or for performing on-chip reactions such as polymerase chain reactions (PCR) for DNA amplification that require elevated temperatures.

Another material property that is important for the *in situ* preparation of monoliths is oxygen permeability. The typical permeability of COC for oxygen is only 0.4 Barrers,[57] which is much less that the value observed for other materials popular for the preparation of microfluidic chips. For example, permeability of PDMS is high reaching to about 10^3 Barrers.[9] This significant difference facilitates the preparation of a monolith within the COC since our polymerization reactions that lead to both surface modification of the channel wall and *in situ* formation of monoliths are usually photo-initiated and proceed *via* a free radical mechanism. These reactions are largely inhibited in the presence of oxygen. This fact makes the oxygen permeability an important metric for the selection of the chip substrates.

Mold insert fabrication

The use of replaceable mold inserts that are mounted directly on the mold base facilitates the rapid prototyping capability of

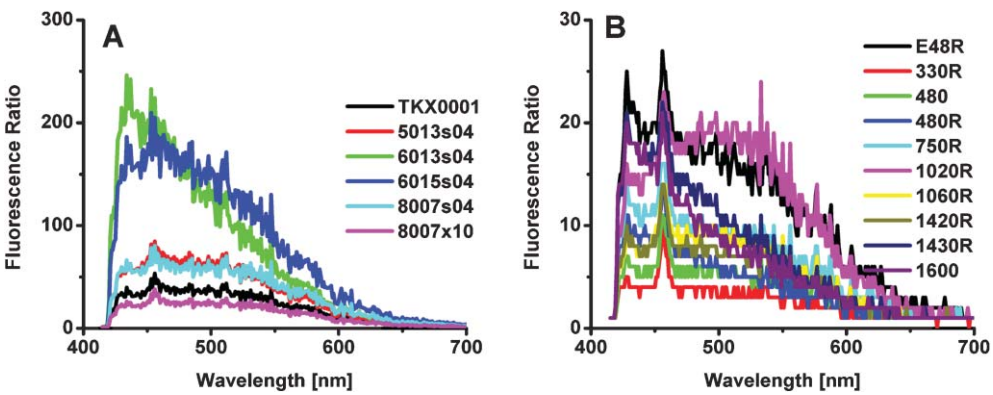

Fig. 2 Fluorescence emission ratio resulting from excitation at 405 nm for various grades of COC from Ticona (A) and Zeon (B). The ratio is obtained by dividing the material fluorescence by that of glass.

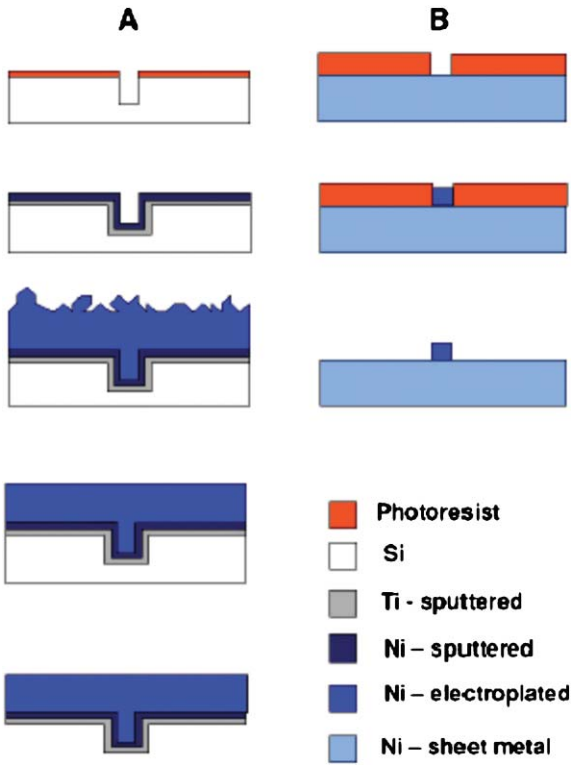

Fig. 3 Fabrication of mold insert by DEEMO (A) and our simplified process (B).

injection molding. Since the inserts contain the channel layout that is transferred to the plastic, this technique allows nearly instantaneous change in the channel layout of the device through a simple replacement of the mold insert.[58] However, the direct mounting of a microfabricated part in the mold cavity requires a very robust and mechanically strong insert that does not wear or deform after many cycles of the high pressure (>100 MPa), clamping force (30 tons), or temperature (250 °C) typical of an injection molding cycle. For this reason LIGA (a German acronym for lithography, electroforming and molding) and DEEMO[59] (dry etch, electroplate, and molding) processes have been developed to produce tough metallic mold inserts. While these processes are widely used, they both suffer from problems such as production of highly stressed parts and long electroplating times. Fabricating an electroform with low internal stress is a very challenging step and several studies have focused on the development of techniques to minimize film stress during electrodeposition.[57,58,60–64] Currently, the electroplating step is the bottleneck in the rapid-prototyping process that severely extends the turnaround time between design of channel layout and final device. In order to truly realize the vision of rapid prototyping we developed a mold insert fabrication process that eliminates the need for overplating, post plating planarization, and electroform film stress. The process steps for the DEEMO process are illustrated schematically in Fig. 3A. Our simplified LIGA process is illustrated in Fig. 3B and begins with spin coating a thick negative-tone resist onto a solid nickel wafer. After lithography, the substrate is electroplated to a thickness that corresponds to the channel height. The resist is then stripped, affording a robust nickel mold. By starting with a solid metal wafer that functions as the base we eliminate the need for overplating and dramatically reduce the thickness of the electroplated film. The electroplating process requires only 8 h to obtain a film 100 μm thick at a current density of 100 A m^{-2}.

Feature uniformity is very important in order to obtain well-defined channels in the chip. To investigate the consistency of the cross-sectional geometry, a mold insert was diced along the channel in increments of 5 mm. An SEM image of a typical channel cross section is illustrated in Fig. 4B. The height and base lengths were recorded for each instance and plotted in Fig. 4A. Clearly, the trapezoidal cross section is maintained and the dimensions vary randomly within a tolerable amount along the entire length of the channel print. The standard deviation of H, W_1, and W_2 are 2, 6, and 4 μm, respectively. This represents another demonstration of the reliability of our process.

Interconnects

Before examining the merits and shortcomings of the basic types of interconnects that have been developed to date it is important to note the numerous requirements for an ideal interconnect: (i) small footprint to allow a high density of fluidic I/O ports, (ii) minimal dead volume, (iii) ease of use, (iv) standard geometry to facilitate interfacing with commercially

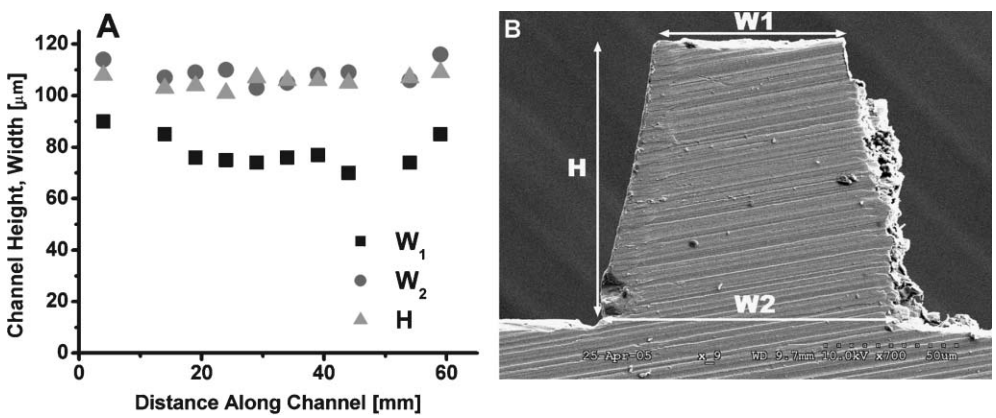

Fig. 4 Cross sectional dimensions of mold insert along the channel (A) and SEM image of typical cross section of mold insert (B).

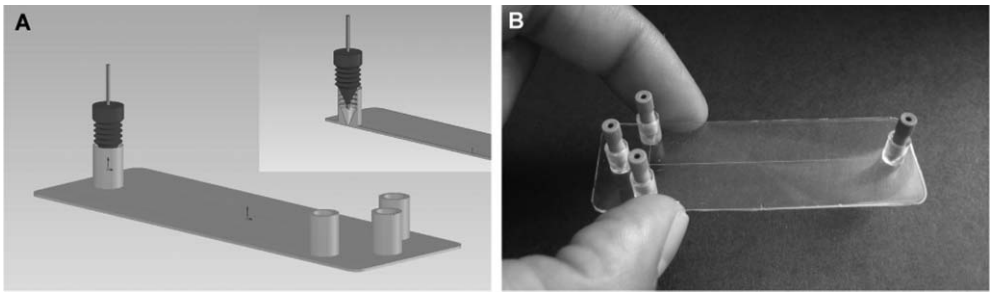

Fig. 5 Concept of microfluidic chip featuring integrated ports (A) and a 4-port microfluidic chip with commercial male fittings threaded integrated ports of an injection molded chip (B).

available devices, (v) reversibility, (vi) reliability, (vii) lack of contamination, and finally, (viii) ease of fabrication.

Microfluidic chips are routinely subjected to high back pressures when the channels are filled with beads. While packed beds are commonplace in large-scale industrial processes, the large surface area they impart has not been widely exploited in microfluidic applications mostly because the chips cannot sustain the high back-pressures required for routine operation. At high pressures, microfluidic devices often fail at one of two junctions: either at the point of attachment of the interconnect, or at the interface between the two bonded parts. Since the bond at the fluidic interconnect is typically weaker than the chip bond we sought to simultaneously eliminate a junction subject to failure and any extra fabrication steps for interconnects, by carefully designing a mold base to produce a part with female ports that are fully integrated into the device. As designed and illustrated in Fig. 5, the upper part of our chip features a hollow boss with ANSI standard internal 6–32 threads located at each fluid entry point.

The need for alignment of the two parts prior to bonding was eliminated by designing the mold base such that all features including ports and channels are integrated in the upper part. The lower half of the chip is completely featureless. Another advantage of forming devices with integrated ports *via* injection molding is that the 2 min injection molding cycle time does not depend on the number of ports. Therefore, this manufacturing technique appears ideal for the construction of high throughput devices that may require many interconnects. The upper limit on interconnect density is determined by the size of commercially available standard male fittings. In addition, the reversible nature of the connection facilitates burst pressure measurements, which we use to quantitatively evaluate the bond strength.

Bonding and burst pressure measurement

Bonding polymer substrates together to hermetically seal the channel with minimal distortion of micrometre-scale features is a very challenging issue that has received considerable attention.[65] The importance of this fabrication step has led to the development of several bonding techniques ranging from simple thermal fusion,[66] gluing,[67] lamination,[68] and solvent bonding[6,80] to more elaborate methods such as laser welding,[69] microwave welding,[65] and resin-gas injection.[70] In order to maintain the chemical homogeneity of all channel walls, we bonded our devices by thermal fusion. The bonding time, temperature, and pressure were varied and the burst pressure was measured for each set of bonding conditions (Table 1). Although the burst pressure is not a direct measure of the bond energy at the interface, it is a valuable engineering parameter that sets the upper limit for device operation.[71]

The burst pressure is measured using chips containing a single channel and two I/O ports. After pumping water into the chip for two minutes, the outlet port is plugged with a standard fitting and the back pressure is recorded. Fig. 6A shows the internal pressure build-up and sudden failure observed in a typical burst pressure measurement. Dramatic device failure occurred by delamination at the bonding interface (Fig. 6B). The results of burst pressure measurements for each bonding condition are presented in Fig. 7. They indicate that the bonding temperature has the most significant effect on bond strength. Bonding at 80 °C affords chips bursting at less than 5 MPa, while a *ca.* 2-fold improvement in bond strength is observed at temperatures of 90 and 95 °C. These temperatures are well above T_g of the material Topas 8007 × 10, measured to be 80 °C by dynamic scanning calorimetry. The strength of the bond achieved by thermal fusion results from chain entanglement of polymer chains located at the surface of the two parts constituting the chip. The chain mobility and therefore their ability to penetrate across the interface is much higher at a temperature above the glass transition. In contrast, bonding pressure seems to have a lesser effect once sufficient pressure is applied to bring the pieces into intimate contact to facilitate chain entanglement. Similarly, bonding time appears to have a small impact beyond a critical minimum time period.

Chips bonded at a temperature of 95 °C and a pressure of 0.28 MPa for 10 min exhibit the best resistance to pressure. As illustrated in Fig. 6, they start to leak at an in-channel pressure of over 12 MPa and burst at 15.6 MPa *i.e.* the highest operational back-pressure of any microfluidic device reported to date. The ability of these chips to sustain such high

Table 1 Bonding parameters for each bonding condition. Each bonding condition was repeated 10 times

Trial	Temperature/°C	Pressure/MPa	Time/min	Yield (%)
1	80	0.47	15	70
2	80	0.47	10	80
3	80	0.71	10	90
4	90	0.24	30	20
5	90	0.28	10	70
6	90	0.36	10	80
7	95	0.28	10	30

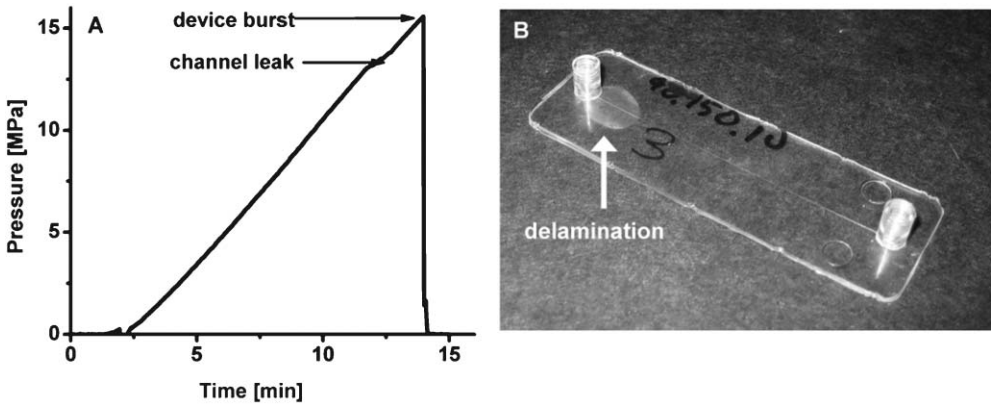

Fig. 6 Pressure build-up and sudden failure by delamination inside a chip bonded using the conditions of trial 7 in Table 1.

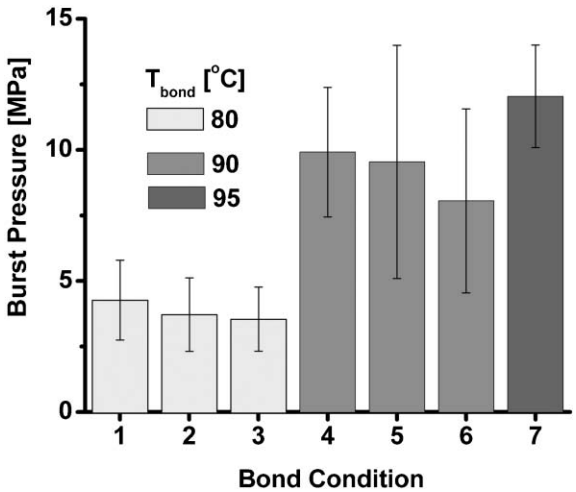

Fig. 7 Average burst pressure for bonding conditions specified in Table 1. Error bars correspond to one standard deviation.

pressures without any observed leakage or break clearly demonstrates the advantage of monolithically integrating interconnects.

Porous polymer monolith in channel

Devices designed for biomedical analysis must be able to perform standard processes such as sample preconcentration, enzymatic digestion, and separation; all of which rely on interaction between the analyte located in the mobile phase and the surface of a solid stationary phase. However, the vast majority of microfluidic devices use open channels that have a small ratio of surface area to channel volume. The limited surface area available for interaction characteristic of such open channel configuration requires the use of longer channels. Although long microfluidic channels can be arranged in a small area by adopting a folded channel configuration, the concomitant turn-induced band broadening severely hinders separation resolution.[72] While dispersive spreading in turns can be corrected by modulating turn geometry[73,74] filling the channels with porous materials that increase surface area has the potential to reduce the required channel length by at least two orders of magnitude.[75]

For decades, chemical engineers have designed macroscale processes that rely on high surface area porous packing materials to conduct a variety of processes including catalysis, adsorption, and separations. Excellent control over the porous and chemical properties of particulate materials in conjunction with a thorough understanding of transport phenomena in packed beds have led to application of this technology to a microfluidic format. Unfortunately, attempts to increase the surface area of microfluidic channels by packing them with porous particles did not afford fully satisfactory results.[54,55,76]

Our solution to increasing the surface area within the channel involves the preparation of a continuous porous polymer monolith that is covalently attached to the walls of the channel.[77] The use of UV light to initiate polymerization reactions directly within the microfluidic channels allows the simple use of a mask to define the exact location of the monolith. *In situ* preparation of monolith begins with injecting a liquid polymerization mixture containing photoinitiator, monomers and porogens into the channel. Upon irradiation with UV light the photoinitiator initiates free-radical polymerization exclusively in the exposed regions.[78]

If the wall of the channel is not chemically modified for covalent attachment, shrinkage of the monolith during polymerization may lead to a void space at the monolith–wall interface.[37] Obviously, any liquid would flow through the large voids exhibiting much lower resistance to flow than the porous polymer. This undesired flow can be avoided by covalently attaching the monolith to the channel wall during the polymerization. Although this attachment is critical to minimize channeling at the monolith–wall interface, several reports describing the preparation of monoliths in plastic chips have omitted any modification step.[43,44,47,49,50] The claim that wall roughness prevents monolith dislodgement ignores the effect that channeling at the monolith–wall interface has, for example on separation efficiency.[44] We have developed a method enabling covalent anchoring of the monolith to the polymer substrates by photoinitiating polymerization reactions directly *from* the channel wall.[79] This approach includes controlled photografting of the walls with ethylene diacrylate that creates a thin layer of polymer with a multiplicity of pendant acrylate groups. These polymerizable vinyl-containing moieties are then incorporated into the monolith during its *in situ* preparation and anchor it to the wall. As illustrated in

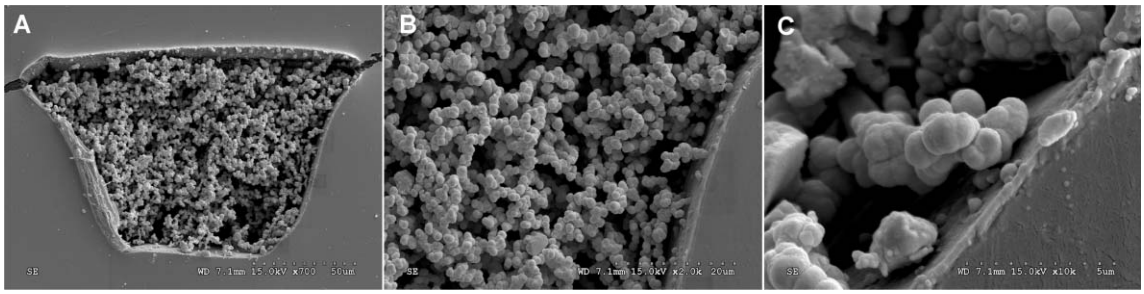

Fig. 8 Cross sectional SEM images of a microfluidic channel containing monolith covalently attached to the wall at magnifications of 600× (A), 2000× (B), and 10 000× (C).

Fig. 8C, the channel was modified to produce a layer about 400 nm thick.

To demonstrate the reactivity of the anchoring layer, we prepared a monolith within our COC chip using a polymerization mixture consisting of butyl methacrylate, ethylene dimethacrylate, decanol and 2,2-dimethoxy-2-phenyl-acetophenone and carried out photopolymerization through a mask. Fig. 8 shows the monolith at various magnifications. The SEM micrographs reveal the globular structure of the monolith with a globule size of about 2 μm as well as large pores among clusters of these globules.

Conclusion

We have designed, developed, and implemented an injection molding process for the fabrication of disposable microfluidic chips with standard, integrated, ready-to-use interconnects that can withstand very high back pressures. In anticipation of detecting analytes *via* LIF we screened several commercially available polymers for low background fluorescence and identified a suitable grade of COC for device production. A robust solid metal mold insert defining the microfluidic channels was rapidly microfabricated using a process that eliminated unnecessary electroplating time. The burst pressure of the chips was measured and used to optimize the bonding conditions enabling an eventual maximum burst pressure of 15.6 MPa. Finally, the suitability of UV transparent high-pressure disposable devices was demonstrated by the *in situ* preparation of a high surface area porous polymer monolith directly within the channels. With devices capable of withstanding such high back pressure we are now able to pursue truly high performance liquid chromatography (HPLC) on-chip. We are also targeting the integration of multiple monolithic modules in a single chip to perform preconcentration, digestion, and separation in the analysis of proteins.

Acknowledgements

Support of this research by a grant of the National Institute of General Medical Sciences, National Institutes of Health (GM-48364) is gratefully acknowledged. The authors also want to acknowledge Nerique Gomez for his assistance with SEM in the National Center for Electron Microscopy, Lawrence Berkeley National Laboratory. This work was supported by the Materials Sciences and Engineering Division of the U.S. Department of Energy under Contract No. DE-AC02-05CH11231. We also thank James Wu of the Materials Sciences Division of Lawrence Berkeley National Laboratory for assistance with substrate annealing for lithography and John Morton of the Department of Mechanical Engineering, University of California at Berkeley for his valuable input regarding the tooling of the mold base.

References

1 D. R. Reyes, D. Iossifidis, P. A. Auroux and A. Manz, *Anal. Chem.*, 2002, **74**, 2623–2636.
2 S. C. Terry, J. H. Jerman and J. B. Angell, *IEEE Trans. Electron Devices*, 1979, **26**, 1880–1886.
3 H. Becker and L. E. Locascio, *Talanta*, 2002, **56**, 267–87.
4 H. Becker and C. Gartner, *Electrophoresis*, 2000, **21**, 12–26.
5 M. A. Roberts, J. S. Rossier, P. Bercier and H. Girault, *Anal. Chem.*, 1997, **69**, 2035–2042.
6 L. J. Kricka, P. Fortina, N. J. Panaro, P. Wilding, G. Alonso-Amigo and H. Becker, *Lab Chip*, 2002, **2**, 1–4.
7 Y. N. Xia and G. M. Whitesides, *Annu. Rev. Mater. Sci.*, 1998, **28**, 153–184.
8 V. Piotter, T. Hanemann, R. Ruprecht and J. HauBelt, *Microsyst. Technol.*, 1997, **3**, 129–133.
9 M. Heckele and W. K. Schomburg, *J. Micromech. Microeng.*, 2004, **14**, R1–R14.
10 B. L. Gray, D. Jaeggi, N. J. Mourlas, B. P. van Drieenhuizen, K. R. Williams, N. I. Maluf and G. T. A. Kovacs, *Sens. Actuators, A*, 1999, **77**, 57–65.
11 K. W. Oh, C. S. Park, K. Namkoong, J. Kim, K. S. Ock, S. Kim, Y. Kim, Y. K. Cho and C. Ko, *Lab Chip*, 2005, **5**, 845–850.
12 C. Gartner, H. Becker, B. Anton and O. Roetting, *Proc. SPIE-Int. Soc. Opt. Eng.*, 2004, **5345**, 159–162.
13 C. K. Fredrickson and Z. H. Fan, *Lab Chip*, 2004, **4**, 526–533.
14 V. Nittis, R. Fortt, C. H. Legge and A. J. de Mello, *Lab Chip*, 2001, **1**, 148–152.
15 D. Figeys, Y. B. Ning and R. Aebersold, *Anal. Chem.*, 1997, **69**, 3153–3160.
16 S. F. Li and C. S. Chen, *IEEE Trans. Adv. Packag.*, 2003, **26**, 242–247.
17 H. Andersson, W. van der Wijngaart, P. Enoksson and G. Stemme, *Sens. Actuators, B*, 2000, **67**, 203–208.
18 A. V. Pattekar and M. V. Kothare, *J. Micromech. Microeng.*, 2003, **13**, 337–345.
19 J. H. Tsai and L. W. Lin, *J. Micromech. Microeng.*, 2001, **11**, 577–581.
20 A. Puntambekar and C. H. Ahn, *J. Micromech. Microeng.*, 2002, **12**, 35–40.
21 T. Yu-Chong and T. J. Yao, *US Pat.*, 6 698 798, 2004.
22 C. H. Chiou and G. B. Lee, *J. Micromech. Microeng.*, 2004, **14**, 1484–1490.
23 A. M. Christensen, D. A. Chang-Yen and B. K. Gale, *J. Micromech. Microeng.*, 2005, **15**, 928–934.
24 H. Chen, D. Acharya, A. Gajraj and J. C. Meiners, *Anal. Chem.*, 2003, **75**, 5287–5291.
25 A. R. Han, O. Wang, M. Graff, S. K. Mohanty, T. L. Edwards, K. H. Han and A. B. Frazier, *Lab Chip*, 2003, **3**, 150–157.

26 M. Brivio, R. E. Oosterbroek, W. Verboom, A. van den Berg and D. N. Reinhoudt, *Lab Chip*, 2005, **5**, 1111–1122.
27 M. Brivio, R. E. Oosterbroek, W. Verboom, M. H. Goedbloed, A. van den Berg and D. N. Reinhoudt, *Chem. Commun.*, 2003, **15**, 1924–1925.
28 B. L. Gray, D. K. Lieu, S. D. Collins, R. L. Smith and A. I. Barakat, *Biomed. Microdevices*, 2002, **4**, 9–16.
29 C. Gartner, H. Becker, B. Anton and O. Roetting, *Proc. SPIE-Int. Soc. Opt. Eng.*, 2004, **5345**, 159–162.
30 P. Aswendt, R. Hofling and S. Gartner, *Proc. SPIE-Int. Soc. Opt. Eng.*, 2005, **5856**, 393–400.
31 Z. Yang and R. Maeda, *J. Chromatogr., A*, 2003, **1013**, 29–33.
32 S. Z. Qi, X. Z. Liu, S. Ford, J. Barrows, G. Thomas, K. Kelly, A. McCandless, K. Lian, J. Goettert and S. A. Soper, *Lab Chip*, 2002, **2**, 88–95.
33 M. Galloway, W. Stryjewski, A. Henry, S. M. Ford, S. Llopis, R. L. McCarley and S. A. Soper, *Anal. Chem.*, 2002, **74**, 2407–2415.
34 R. Jurichaka, C. Blattert, C. Tahhan, A. Muller, A. Schoth and W. Menz, *Proc. SPIE-Int. Soc. Opt. Eng.*, 2005, **5718**, 65–72.
35 V. Galhotra, C. Marques, Y. Desta, K. Kelly, M. Despa, A. Pendse and J. Collier, *Proc. SPIE-Int. Soc. Opt. Eng.*, 2005, **2879**, 168–173.
36 J. Tuma, PhD thesis, Louisiana State University, 2003.
37 T. B. Stachowiak, T. Rohr, E. F. Hilder, D. S. Peterson, M. Q. Yi, F. Svec and J. M. J. Fréchet, *Electrophoresis*, 2003, **24**, 3689–3893.
38 W. Ehrfeld, V. Hessel, H. Lowe, C. Schulz and L. Weber, *Microsyst. Technol.*, 1999, **5**, 105–112.
39 A. M. Tan, S. Benetton and J. D. Henion, *Anal. Chem.*, 2003, **75**, 5504–5511.
40 Y. Yang, C. Li, J. Kameoka, K. H. Lee and H. G. Craighead, *Lab Chip*, 2005, **5**, 869–876.
41 J. Choi, S. Kim, R. Trichur, H. Cho, A. Puntambekar, R. L. Cole, J. R. Simkins, S. Murugesan, K. Kim, J. Lee, G. Beaucage, J. H. Nevin and C. H. Ahn, *Proc. μTAS*, 2001, 411–412.
42 A. Piruska, I. Nikcevic, S. H. Lee, C. Ahn, W. R. Heineman, P. A. Limbach and C. J. Seliskar, *Lab Chip*, 2005, **5**, 1348–154.
43 J. Kameoka, H. G. Craighead, H. W. Zhang and J. Henion, *Anal. Chem.*, 2001, **73**, 1935–1941.
44 Y. N. Yang, C. Li, K. H. Lee and H. G. Craighead, *Electrophoresis*, 2005, **26**, 3622–3630.
45 D. S. Lee, H. Yang, K. H. Chung and H. B. Pyo, *Anal. Chem.*, 2005, **77**, 5414–2540.
46 P. Mela, A. van den Berg, Y. Fintschenko, E. B. Cummings, B. A. Simmons and B. J. Kirby, *Electrophoresis*, 2005, **26**, 1792–1799.
47 C. Li, Y. N. Yang, H. G. Craighead and K. H. Lee, *Electrophoresis*, 2005, **26**, 1800–1806.
48 D. Nilsson, S. Balslev and A. Kristensen, *J. Micromech. Microeng.*, 2005, **15**, 296–300.
49 Y. N. Yang, J. Kameoka, T. Wachs, J. D. Henion and H. G. Craighead, *Anal. Chem.*, 2004, **76**, 2568–2574.
50 J. Gaudioso and H. G. Craighead, *J. Chromatogr., A*, 2002, **971**, 249–253.
51 I. Gusev, X. Huang and C. Horvath, *J. Chromatogr., A*, 1999, **855**, 273–290.
52 K. R. Hawkins and P. Yager, *Lab Chip*, 2003, **3**, 248–252.
53 H. K. Wu, T. W. Odom, D. T. Chiu and G. M. Whitesides, *J. Am. Chem. Soc.*, 2003, **125**, 554–559.
54 R. D. Oleschuk, L. L. Shultz-Lockyear, Y. B. Ning and D. J. Harrison, *Anal. Chem.*, 2000, **72**, 585–590.
55 A. B. Jemere, R. D. Oleschuk, F. Ouchen, F. Fajuyigbe and D. J. Harrison, *Electrophoresis*, 2002, **23**, 3537–3544.
56 C. H. Hidrovo and D. P. Hart, *Meas. Sci. Technol.*, 2001, **12**, 467–477.
57 S. Basrour and L. Robert, *Mater. Sci. Eng., A: Struct.*, 2000, **288**, 270–274.
58 Y. Tsuru, M. Nomura and F. R. Foulkes, *J. Appl. Electrochem.*, 2000, **30**, 231–238.
59 J. Elders, H. V. Jansen, M. Elwenspoek and W. Ehrfeld, *IEEE MEMS Proc.*, MEMS '95 Meeting, Amsterdam, 29th January–2nd February 1995, IEEE Publisher, New York, 1995, pp. 238–243.
60 Y. Tsuru, M. Nomura and F. R. Foulkes, *J. Appl. Electrochem.*, 2002, **32**, 629–634.
61 P. T. Tang, *Electrochim. Acta*, 2001, **47**, 61–66.
62 Z. J. Wei, Y. Y. Wang, C. C. Wan and C. H. Huang, *Mater. Chem. Phys.*, 2000, **63**, 235–239.
63 K. C. Chan, N. S. Qu and D. Zhu, *J. Mater. Process. Technol.*, 1997, **63**, 819–822.
64 B. Kebabi and C. K. Malek, *J. Vac. Sci. Technol., B*, 1991, **9**, 154–161.
65 A. A. Yussuf, I. Sbarski, J. P. Hayes, M. Solomon and N. Tran, *J. Micromech. Microeng.*, 2005, **15**, 1692–1699.
66 R. T. Kelly and A. T. Woolley, *Anal. Chem.*, 2003, **75**, 1941–1945.
67 H. K. Wu, B. Huang and R. N. Zare, *Lab Chip*, 2005, **5**, 1393–1398.
68 C. L. do Lago, H. D. T. da Silva, C. A. Neves, J. G. A. Brito-Neto and J. A. F. da Silva, *Anal. Chem.*, 2003, **75**, 3853–3858.
69 J. W. Chen and J. M. Zybko, *Proc. SPIE-Int. Soc. Opt. Eng.*, 2005, **5718**, 92–98.
70 S. Y. Lai, X. Cao and L. J. Lee, *Anal. Chem.*, 2004, **76**, 1175–1183.
71 S. Satyanarayana, R. N. Karnik and A. Majumdar, *J. Micro-electromech.*, 2005, **14**, 392–399.
72 S. K. Griffiths and R. H. Nilson, *Anal. Chem.*, 2000, **72**, 5473–5482.
73 B. M. Paegel, C. A. Emrich, G. J. Weyemayer, J. R. Scherer and R. A. Mathies, *Proc. Natl. Acad. Sci. U. S. A.*, 2002, **99**, 574–579.
74 S. K. Griffiths and R. H. Nilson, *Anal. Chem.*, 2001, **73**, 272–278.
75 This calculation was made using a specific surface area of 10 m^2 g^{-1} for typical methacrylate-based monolith placed in a channel 100 μm deep and 100 μm wide.
76 G. Ocvirk, E. Verpoorte, A. Manz, M. Grasserbauer and H. M. Widmer, *Anal. Methods Instrum.*, 1995, **2**, 74–82.
77 F. Svec and J. M. J. Fréchet, *Science*, 1996, **273**, 205–211.
78 C. Viklund, E. Ponten, B. Glad, K. Irgum, P. Horstedt and F. Svec, *Chem. Mater.*, 1997, **9**, 463–471.
79 T. Rohr, D. F. Ogletree, F. Svec and J. M. J. Fréchet, *Adv. Funct. Mater.*, 2003, **13**, 264–270.
80 J. J. Shah, J. Geist, L. E. Loascio, M. Gaitin, M. V. Rao and W. N. Vreeland, *Anal. Chem.*, 2006, **78**, 3348–3353.

